Limit Cycling in Control of Underwater Vehicles Caused by Lossy Quantized Communication Channels

Eric Gilbertson and Franz Hover
Department of Mechanical Engineering
Massachusetts Institute of Technology
Cambridge, Massachusetts 02139
Email: egilbert@mit.edu, hover@mit.edu

Abstract— **Many multi-agent robotic applications such as pursuit and monitoring depend heavily on wireless communications, whose performance can impact the whole system. We derive here a closed-form describing function for a combined quantizer, binary erasure channel, and linear filter decoder for a SISO system; this combination is a fundamental model in wireless feedback control, and has wide practical relevance. Describing functions identify limit-cycles in nonlinear systems, and thus the result allows us to rapidly characterize the dynamic precision of wirelessly-controlled systems. The key steps in our derivation can be applied to other fundamental systems, and we derive describing functions for systems where the linear filter element is replaced with zero-output and hold-output decoders. Analysis of these systems using the describing function technique is orders of magnitude faster than Monte Carlo simulation.**

I. INTRODUCTION

Wirelessly connected robotic systems have become widespread in the terrestrial, aerial and underwater environments. As one would expect, demand on throughput grows to fill the available channel capacity; in a clean short-range RF setting, entire images may be transferred in each cycle, as part of a vision-based control system, whereas in the ocean, acoustic channels with twenty bps allow only the most basic sensor and command information to be shared regularly. At the same time, packet-based wireless communication systems operating near their limits are necessarily quantized, and prone to loss. This directly impacts the overall system performance, and therefore methodologies for understanding and designing feedback systems with quantization and packet loss are valuable.

Tsumura *et al.* [1] developed one of the first fundamental analyses for this problem, and Niu *et al.* [2] later derived a set of linear matrix inequalities that guarantee feedback stability for packet loss and quantization in the sensor channel. This result was extended by Liu *et al.* [3] to include quantization and packet loss also in the controller channel; Dai [4] added random delays. Rasool and Nguang [5] recently introduced a variation where disturbance-to-penalty norm can be minimized. The stability guarantees in these works, however, tend to rely on infinite-length logarithmic quantizers.

Our main goal in this paper is to analyze limit cycles – i.e., self-induced oscillations in nonlinear systems - that are induced by quantization and packet loss within a feedback loop. Limit cycles are central in the performance of robotic and other systems because they dictate the precision which can be achieved.

There are three main methods to find limit cycles: Bendixson's theorem, contraction, and describing functions. Bendixson's Theorem states that if a region of state space has no trajectories leaving it, then trajectories must go to limiting sets, which are either equilibrium points or limit cycles [6]. The theorem has been used to prove stability of some systems such as biological cellular concentrations [7] and formation-keeping for mobile agents [8]. However, it does not give insights into the limit cycle characteristics. Contraction theory is similar to Bendixson's theorem in many ways, and states that a system moves to a unique trajectory when initial conditions or disturbances are forgotten exponentially fast. Contraction has been used, for instance, to study limit-cycling of coupled nonlinear oscillators [9].

A describing function (DF) is a quasi-linear approximation to a nonlinear element, and usually depends explicitly on the form of its input; for sinusoidal signals in a limit cycle, the DF depends on the input frequency or amplitude, or both [10]. DF's have been used successfully in many applications. To name a few, in electrical engineering Sanders [11] studied limit cycles in periodically-switched circuits, and Peterchev *et al.* [12] found quantization conditions that eliminate limit cycles in digitally-controlled PWM converters. In control, E. Kim *et al.* [13] developed a DF for a fuzzy logic controller. In ocean engineering, Yoerger *et al.*[14] used DF's to characterize limit cycles in underwater robots caused by nonlinear thruster dynamics. More recently, DF's have been widely applied to stability analysis of airfoils (e.g., Tang *et al.* [15]) and flame formation in combustion (Noiray *et al.*[16]). Gelb and Vander Velde [10] provide a good resource, with many other DF's for a wide range of applications. It is noteworthy that these prior works all address DF's for hardware and physical elements, but not for *information sent across channels*, our current focus. The present work is also unique in that the dynamic element whose describing function is to be developed is itself stochastic.

Describing functions can identify limit cycles in a number of communication-constrained robotic tasks, including remote-sensed and multi-vehicle positioning systems, and contact manipulation. In the case of acoustic communications

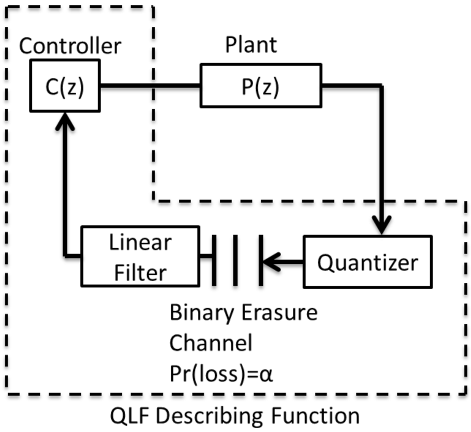

Fig. 1: Block diagram for control system with quantizer, binary erasure channel, linear filter decoder, and LQR controller. The input to the QLF DF is a single sensor signal, and the output a single control command. We assume an LQR-like controller with a constant gain.

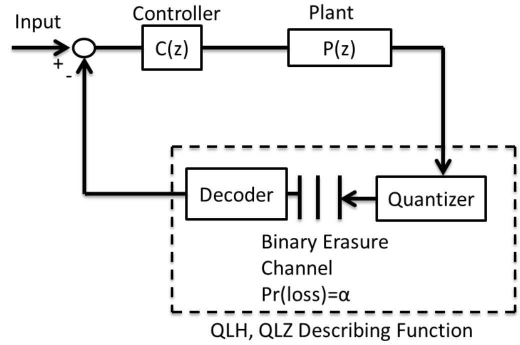

Fig. 2: Block diagram for control system with quantizer, binary erasure channel, and decoder. For the QLH system the decoder is a hold-output, and for the QLZ system the decoder is zero-output.

underwater, quantization levels can be high and thus limit cycles quite pronounced, as we will demonstrate.

We first develop a single describing function for the canonical scenario of a quantizer on the plant output, a binary erasure channel, a linear-filter state estimator and an LQR controller for a SISO system, as shown in Figure 1. In this system the input to the DF is a single sensor measurement, and the output a single control command. We refer to this scenario by the acronym QLF. In practice, the quantization level affects packet loss rate for a given operation, and we can directly couple the quantizer and lossy-channel DF's. The result is a clean analytical description for the canonical problem. We then apply the same derivation technique to develop a DF for the case where the linear filter is replaced with a hold-output decoder, and finally note the trivial case of a zero-output decoder. We refer to the former case as QLH, and to the latter as QLZ. Both QLH and QLZ cases describe only the channel and decoder, and can thus be applied to a lossy sensor channel or lossy controller channel. These three cases represent the baseline approaches taken in many control systems, and hence our analysis is highly relevant to current practice. The DF's we develop are orders of magnitude faster in identifying limit cycles than are Monte Carlo simulations.

We derive the above SISO describing functions in Sec. II. We verify the analytical results via simulation in Section III, and show the DF for a standard linear quantizer in Section IV. We combine the DF's with a standard linear quantizer DF in Sec. V and show a numerical example of how to use the new DF's to find limit cycles in Sec. VI. We conclude with Sec. VII.

II. Describing Function Solutions

A. Loss with LQG-type Controller

We first derive a DF for the case of a binary-erasure channel with a linear filter and LQR controller, as shown in Figure 1. We assume single sensor input signal of the form $a\sin(\omega kdt)$, for amplitude a, input frequency ω, sampling timestep dt, and timestep number k. We model the binary erasure channel with a Bernoulli variable θ_k indicating whether the signal was successfully received at time step k, and the linear filter state estimate with variable F_k giving the output signal at timestep k. θ_k is given by

$$\theta_k = \begin{cases} 1, & \text{if transmission success, probability } 1-\alpha \\ 0, & \text{if transmission failure, probability } \alpha \end{cases} \tag{1}$$

For the LQG-type controller we use the following algorithm, based on standard discrete-time filtering. Propagate forward in time with $\hat{x}_{k|k-1} = A\hat{x}_{k-1|k-1} + Bu_{k-1}$ where x_k is the state estimate at timestep k and A, B are constant system matrices. If the signal is received, update the estimate with $\hat{x}_{k|k} = \hat{x}_{k|k-1} + K_f\left(z_k - C\hat{x}_{k|k-1}\right) = (I - K_fC)\hat{x}_{k|k-1} + K_f z_k$ where K_f is the filter gain matrix, z_k is the measurement, and C is a constant output matrix. Because K_f is constant in this algorithm, it is assumed that the effects of packet-loss have already been accounted for, or that they are minor; the design of a fixed K_f for lost packets is outside the present scope. If the signal is not received, we perform no update: $\hat{x}_{k|k} = \hat{x}_{k|k-1}$. Finally, the control command is $u_k = K_u\hat{x}_{k|k}$, where K_u is a constant gain matrix.

Defining $F_k \doteq \hat{x}_{k|k}$ and $G \doteq A + BK_u$, if the input signal to the controller takes the specific limit-cycle form $z_k = a\sin(\omega kdt)$, then we can easily derive

$$\begin{aligned} F_k \quad = \quad & \theta_k\left[(I - K_fC)GF_{k-1} + K_f a\sin(\omega kdt)\right] + \\ & (1-\theta_k)GF_{k-1} \end{aligned} \tag{2}$$

In accordance with the describing function method, we assume the output control signal can be approximated by a sine wave with a different amplitude and phase shift, given by

$$D_k = A_{lf}\sin(\omega(kdt - T_{lf})). \tag{3}$$

The "lf" subscript denotes that we are including a loss and a controller of the LQG-type – having a a filter update in particular. To visualize this describing function we show the behavior of an example two-state LQG-like controller in Figure 3 (top plot). This example is analyzed in more detail in Section III-A.

The describing function that best approximates the output signal is the one with the smallest squared-error between expected output and describing function. This is the optimization problem

$$\min_{A_{lf},T_{lf}} J \text{ , where } J \doteq E\left[\sum_{k=1}^{f}\left(D_k(A_{lf},T_{lf}) - K_u F_k\right)^2\right].$$

Here f is the number of time steps the minimization is taken over; clearly f has to be a large number for accuracy reasons, but we will show that practical results are still easy to obtain. Solving this minimization yields clean analytic solutions for A_{lf} and T_{lf}:

$$\boxed{T_{lf} = \frac{1}{\omega}\arctan(z)} \tag{4}$$

$$\text{where } z = \frac{K_u(K_4K_3 - K_2K_5 - K_1K_5)}{K_u(K_3K_5 + K_2K_4 - K_1K_4)} \tag{5}$$

$$\boxed{\frac{A_{lf}}{a} = \frac{K_u(K_5 - K_4 z)\sqrt{1+z^2}}{-K_3z^2 - 2K_2 z + K_3}} \tag{6}$$

and $K_1,\ldots,K_5$ are specific functions of the underlying parameters ω, dt, f, α, etc. These derivations are to be shown in a forthcoming paper.
Because this is the unique solution to an unconstrained problem, we conclude that global optimality is achieved.

B. Loss with Hold-Output

We next consider a binary-erasure channel and hold-input decoder, as shown in Figure 2, again assuming an input signal of the form $a\sin(\omega k dt)$. In contrast with the LQG-like case above, the DF now contains only the lossy channel and the hold-input; the controller is grouped with the plant.

As before, we model the binary erasure channel with a Bernoulli variable θ_k indicating whether the signal was successfully received at time step k, and the hold-input decoder with variable H_k giving the output signal at timestep k. H_k is given recursively by

$$H_k = \theta_k a\sin(\omega k dt) + (1-\theta_k)H_{k-1} \tag{7}$$

As before, we assume the output signal can be approximated by a sine wave DF with a different amplitude and phase shift, given by A_{lh} and ωT_{lh}.

Figure 3 (middle plot) shows an empirical example of how such a DF approximates a decoded signal for an input sine wave sent through a binary erasure channel. In this simulation packet loss is set to ninety percent. Because the output is given by a hold-output rule, the average value of the output is well-approximated by a delay and a non-unity gain.

We can derive the DF for this channel/decoder system by treating it as a special case of the LQG-like model of the previous section. If we set the sensor noise R_k to zero and the filter gain K, C, and G matrices to the identity matrices, then the linear filter equation (2) reduces to the hold-output decoder equation (7). Following a similar derivation as for A_{lf} and T_{lf}, we find

$$\boxed{T_{lh} = \frac{1}{\omega}\arctan(z')} \tag{8}$$

$$\text{where } z' = \frac{K_4'K_3 - K_2K_5' - K_1K_5'}{K_3K_5' + K_2K_4' - K_1K_4'}, \text{ and} \tag{9}$$

$$\boxed{\frac{A_{lh}}{a} = \frac{(K_5' - K_4'z')\sqrt{1+z'^2}}{-K_3z^2 - 2K_2 z + K_3}} \tag{10}$$

where K_1, K_2, and K_3 are as above, and there are two new scalars K_4' and K_5' which also depend on the same system parameters.

C. Loss with Zero Output

The zero-output decoder outputs the input signal if the packet transmission is successful, and outputs zero if the packet is unsuccessful. This setup is represented in Figure 2. The model is simply

$$Z_k = \theta_k a\sin(\omega k dt) \tag{11}$$

This describing function has the parameters

$$\boxed{\frac{A_{lz}}{a} = 1-\alpha} \text{ and } \boxed{T_{lz} = 0} \tag{12}$$

Figure 3 (bottom plot) shows an example case of the decoded signal out the zero-output controller when an input signal is sent through a channel with 50% packet loss.

For the DF's to be valid we require that at least one period of the input signal is sampled and that at least four samples are taken per period. This leads to the inequalities

$$\frac{2\pi}{f} < \omega dt < \frac{\pi}{2} \tag{13}$$

For $f = 1000$ this restricts our input nondimensional frequencies to be in the range $10^{-2.2}$ to $10^{0.2}$ Figure 4 shows the values of T_{lh} for a range of f between 100 and 1000 at frequency $\omega dt = 0.1$, for a range of packet loss probabilities. The plot shows eventual convergence for large values of f, and justifies a choice of $f = 1000$ for subsequent computations. Similar convergence is seen in plots of A and different input frequencies, and for different values of f in the zero-output DF and LQG DFs we consider. Much larger values of f lead to longer computation times with similar accuracy of results.

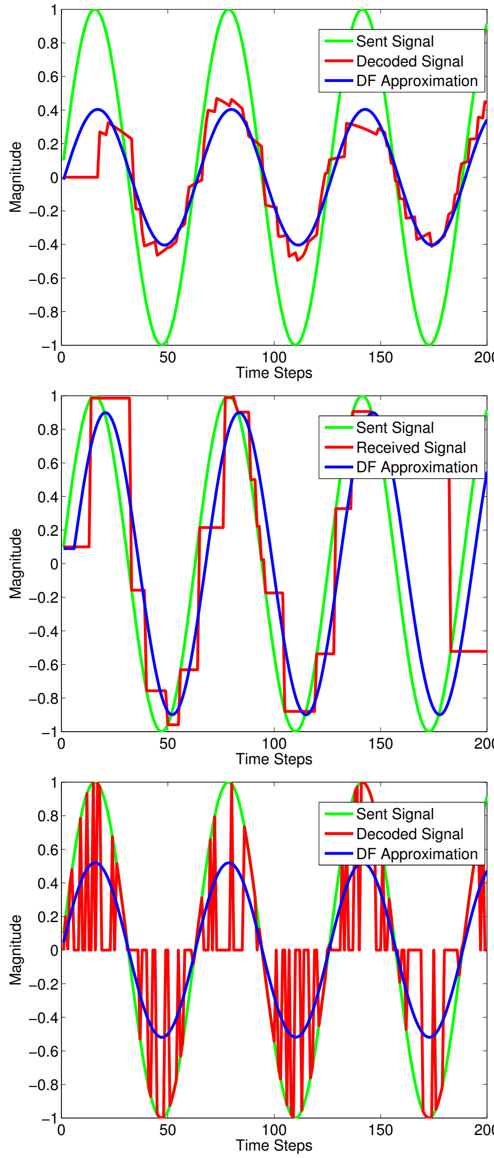

Fig. 3: Comparison of LQG DF (top), hold-output DF (middle), and zero-output DF (bottom) derived by Monte Carlo simulation with input and decoded signals. For LQG DF, system has 70% packet loss as detailed in Section III-A. The optimal parameters values are found to be gain $A = 0.40$ and delay $T = 0.14$ time steps. For hold-output DF, system has 90% packet loss, and optimal parameters values are gain $A = 0.9$ and delay $T = 8$ time steps. For zero-output DF, system has 50% packet loss, with optimal gain $A = 0.5$

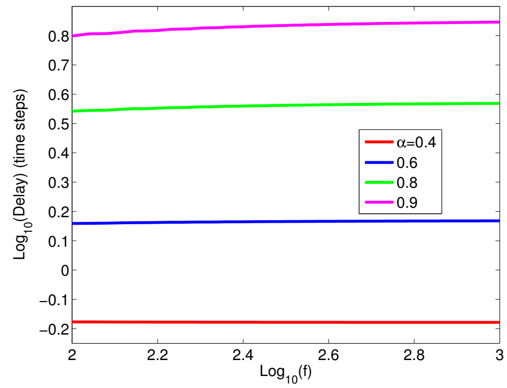

Fig. 4: Convergence of analytically-determined value of hold-output phase for increasing values of f, different values of α, and $\omega dt = 0.1$.

III. Model Verification

A. LQG Describing Function

To visualize the LQG DF case we analyze a specific plant and controller example. We consider a two-state mass-spring-damper system with mass position controlled by an applied force, and only position feedback. This example is a simple model of a robotic contact task. The example system is described by the equation

$$m\ddot{x} + b\dot{x} + kx = F \tag{14}$$

where m is the mass, b is the damper coefficient, k is the spring constant, and F is the force applied by the controller. We use the values $m = 4$, $b = 2$, and $k = 1$, with LQR controller gain matrix $[-0.38 - 0.86]$, constant linear filter gain matrix $[0.5 \ \ 0.1]$. The closed-loop step response of the mass position over time with the gains chosen, for a time step of $dt = 0.1$ seconds, has a damping ratio of 0.4 and a natural frequency of 0.38 rad/sec. For this example we discretized the system model using zero-order hold, with the filter in discrete time.

In Figure 3 (top plot) we show an example time response of this system with a sinusoidal input and lossy sensor feedback channel. We plot a case with 70% packet loss, for parameter values $\omega = 1$, $a = 1$.

We plot the values of the analytically-derived DF gain and phase in Figure 5 from the position measurement signal to control command for a range of input frequencies and packet loss rates, with analytical results verified by simulation at several different input frequencies.

B. Hold-Output Describing Function

To verify the hold-output DF we run a Monte Carlo simulation and curve fit to find the optimal values of A_{lh} and T_{lh} for a given packet loss rate, input frequency, time step size, and number of time steps. Note that this DF does not depend on a model, unlike the LQG DF, and is hence a universal description, parametrized only by f.

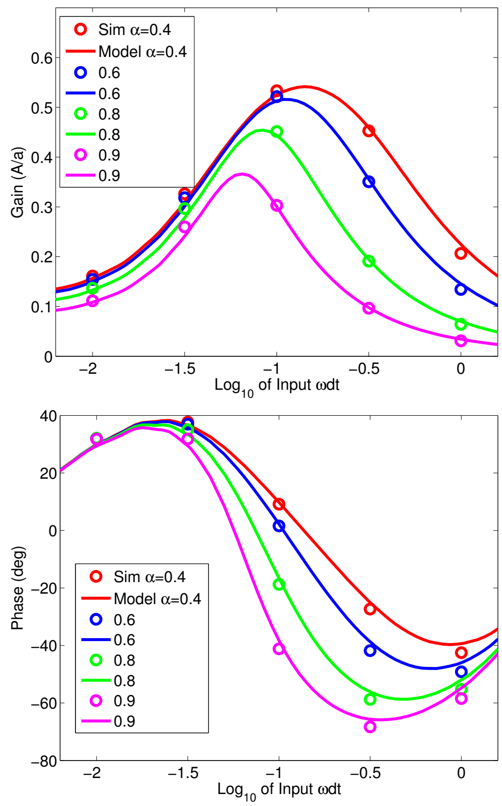

Fig. 5: LQG DF gain (top plot) and phase (bottom plot) from analysis and Monte Carlo simulation, for the contact task example.

We plot the values of A_{lh} and T_{lh} for a range of packet loss rates and input frequencies in Figure 6 and see good agreement between model and simulations.

IV. Quantizer Describing Functions

Quantizers have well-known describing functions [10]. We consider a uniform round-off quantizer with quantization bin size h and input amplitude a. The quantizer is characterized by the describing function $N(a/h)$, given by

$$N\left(\frac{a}{h}\right) = \frac{4h}{\pi a}\sum_{i=1}^{n}\sqrt{1-\left(\frac{(2i-1)h}{2a}\right)^2} \qquad (15)$$

$$\frac{2n-1}{2} < \frac{a}{h} \leq \frac{2n+1}{2}$$

where n is an integer defining which quantization bin a/h is in. The logarithmic quantizer DF is very similar to that of the uniform quantizer and therefore our analysis is also extensible to logarithmic quantizers.

This DF is only dependent on the input amplitude, not frequency. Figure 7 shows the uniform quantizer DF gain as a function of the ratio of input amplitude to quantization bin size a/h. As the ratio a/h increases, the quantization becomes finer and the gain approaches unity.

To restrict the independent variables further, we assume an exponential relationship between quantization level and

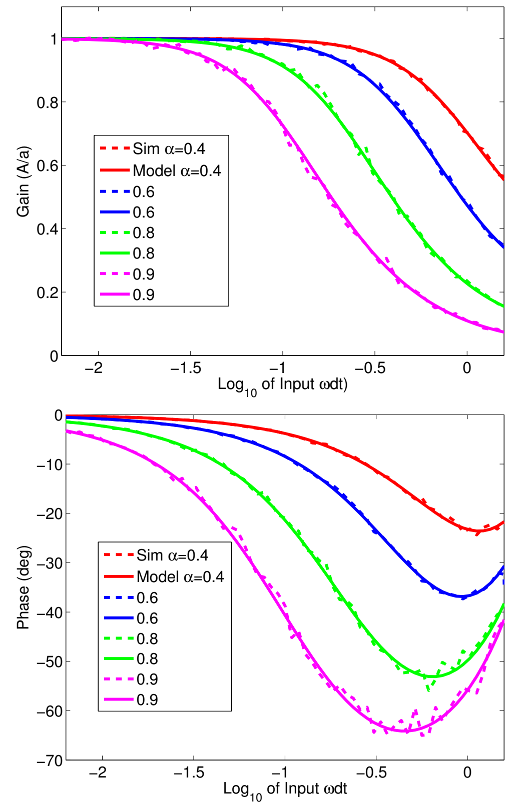

Fig. 6: Comparison of analytic hold-output model (solid lines) of gain (top plot) and phase ωT (bottom plot) to Monte Carlo simulation (dashed lines) for a range of input frequencies and packet loss rates.

packet loss [17] given by $\alpha = e^{-mh}$, where h is the size of quantization bins and m is a parameter to be tuned to match the environmental conditions and the system. This expression means that very fine quantization, i.e. small values of h, lead to higher packet loss rates. Coarse quantization, i.e. larger values of h, lead to lower packet loss rates. We will assume $m = 1/20$ for the rest of this paper.

V. Combined Quantizer and Channel-Decoder Describing Functions

A. QLF

The quantizer DF is independent of input frequency and the LQG DF is independent of input amplitude. Thus the two functions can be cascaded into one (QLF). Assuming a uniform quantizer, the QLF DF has a gain of $N(a/h)A$ and a phase of $-\omega T_F$, where $N(a/h)$ is given by equation (15), A_F is given by equation (6), and T_F is given by equation (4). Thus, for a given packet loss probability α, the combined DF has gain

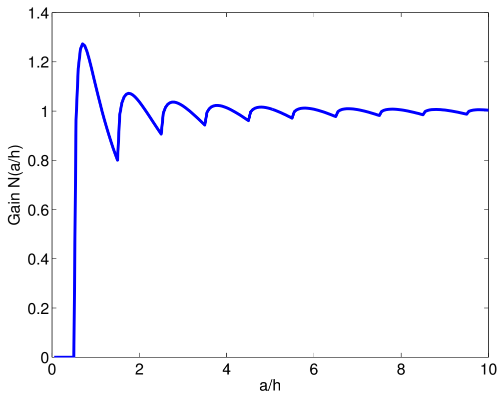

Fig. 7: Describing function gain $N(a/h)$ for uniform quantizer [10] with bin width h and input signal amplitude a.

$$\left(\frac{(K_5 - K_4 z)\sqrt{1+z^2}}{-K_3 z^2 - 2K_2 z + K_3}\right)\frac{-4\ln(\alpha)}{m\pi a} \times \sum_{i=1}^{n}\sqrt{1-\left(\frac{(2i-1)\ln(\alpha)}{2am}\right)^2} \quad (16)$$
$$\frac{2n-1}{2} < \frac{a}{h} \leq \frac{2n+1}{2}$$

This QLF DF has several parameters that will be determined by the application. The factor m relating quantization level to packet erasure will be determined by the channel. Quantization bin size h relative to input amplitude a would be a design choice, and the parameter f would be determined by computational power available and accuracy desired.

Figure 8 shows a plot of gain versus quantization level for the QLF DF, for different input frequencies and input magnitudes a, for the contact task model.

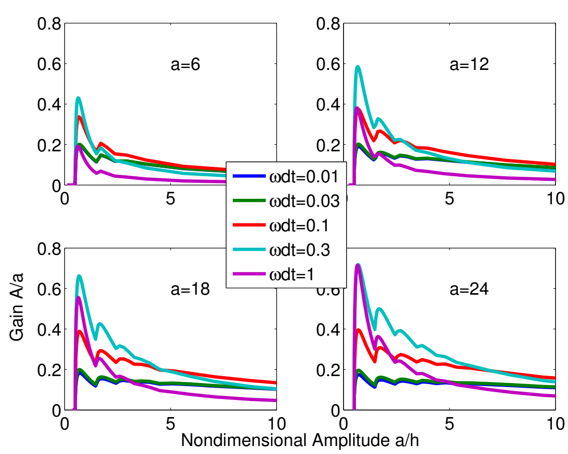

Fig. 8: QLF magnitude as a function of input frequency, quantization, and input amplitude for the contact task model.

B. QLH

We next investigate the gain and phase of the QLH DF with a uniform quantizer. The equation for this DF is identical to that of the QLF DF except the coefficients K_4, K_5, and z are replaced by K_4', K_5', and z'. Figure 10 shows a plot of gain versus quantization level for different input frequencies and different input magnitudes a.

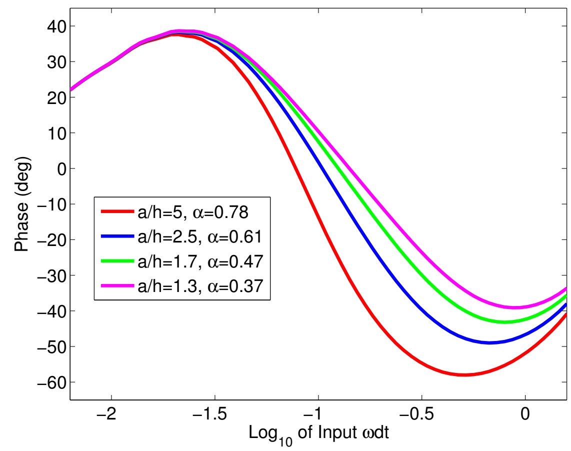

Fig. 9: QLF phase as a function of input frequency and quantization for the contact task model. This is a variation of the bottom plot of Figure 5, with the $\alpha - h$ map imposed.

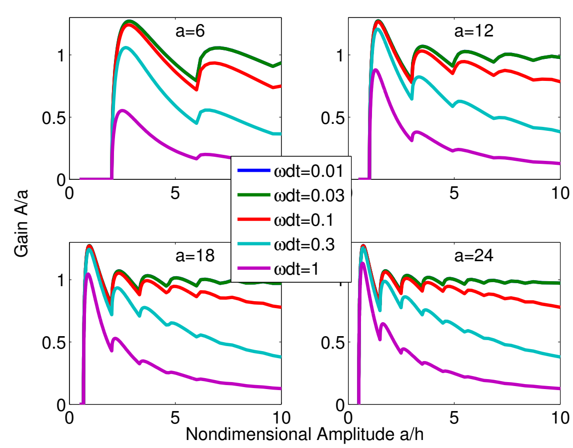

Fig. 10: QLH magnitude as a function of input frequency, quantization, and input amplitude. Frequencies are in rad/sec.

Figure 11 plots the output phase as a function of input frequency for different quantization levels. The magnitude of the phase decreases with coarser quantization (larger h), likely because fewer packets are dropped and thus the hold-input has a smaller effect of delaying the signal. The phase is likely close to zero at low input frequencies because many samples are taken per period, leading to a closer approximation between the hold-input and signal and thus smaller delays for the DF.

C. QLZ

The QLZ DF magnitude is given by the expression

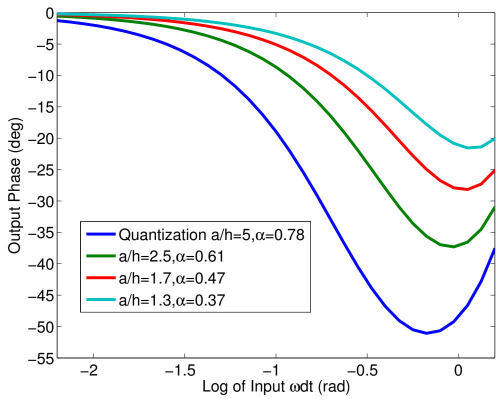

Fig. 11: QLH phase as a function of input frequency and quantization. This is a variation of the bottom plot in Figure 6, with the $\alpha - h$ map imposed.

$$(1-\alpha)\frac{-4\ln(\alpha)}{m\pi a}\times\sum_{i=1}^{n}\sqrt{1-\left(\frac{(2i-1)\ln(\alpha)}{2am}\right)^2} \tag{17}$$
$$\frac{2n-1}{2}<\frac{a}{h}\le\frac{2n+1}{2}$$

We plot the magnitude of the QLZ DF as a function of input amplitude and quantization in Figure 12. This plot shows that the magnitude is always less than one, in contrast to the magnitudes of the QLH plots. This is because the zero-control action always acts to reduce the magnitude of the decoded signal compared to the input signal.

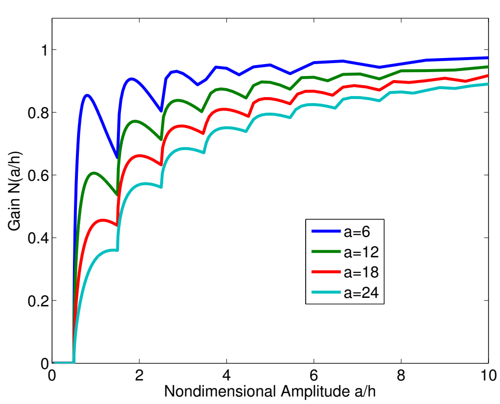

Fig. 12: QLZ magnitude as a function of quantization and input amplitude.

VI. Limit Cycle Numerical Example

The QLF, QLH, and QLZ DFs can be used to find limit cycles in dynamic systems. As an example, we consider a simple double integrator system with position sensor signal quantized and sent through a lossy channel before being decoded and sent to a controller. This example is not unlike a scenario where an underwater robot must maintain a constant range to a leader, where the range measurement is quantized and lossy. We consider four different setups in this example: the sensor signal is passed through a QLZ, QLH, QLF, or pure quantizer (Q) block. To fairly compare the different DF's, we first design LQR and Kalman gains in continuous time for an LQG controller/filter to be used in the QLF system. We use the transfer function of the LQG controller/filter from the sensor measurement to the control output as the compensator transfer function for the QLZ and QLH systems. This way, in continuous time in the absence of packet loss and quantization, the systems are equivalent.

We assume that the actual system operates in discrete time and the sensor measurement is subject to a one-timestep delay of 0.1 seconds, leading to a closed-loop response that is more oscillatory than originally designed, but still stable. We then show that, if the sensor signal is lossy and quantized, as in a real underwater robotic control system, the QLZ, QLH, QLF, and Q blocks predict limit cycles in the otherwise stable system. The limit cycle plots of these scenarios could be used as a tool to pick quantization levels that result in no or fewer limit cycles, or that result in limit cycles with smaller amplitudes. The plots can also determine which controller scheme results in fewer or no limit cycles.

We first consider the QLF system and design LQR and Kalman gains in continuous time. The equivalent transfer function from sensor output to control signal for our chosen gains is given by

$$T(s)=\frac{3371s+10^4}{s^2+35.02s+563.1} \tag{18}$$

In relation to Figures 1 and 2, T(s) represents all elements excluding the plant in the case of no quantization and no packet loss. The closed-loop step response of this system in continuous time is shown in Figure 13. Figure 14 shows

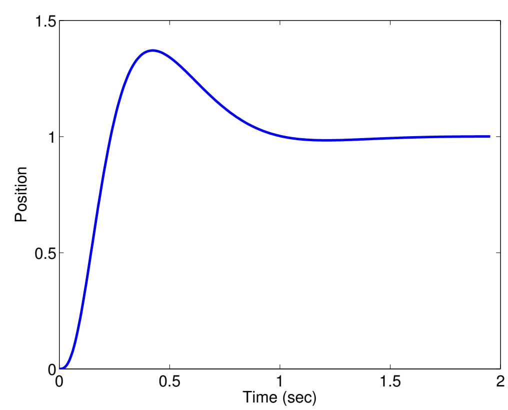

Fig. 13: Closed-loop step response of example system in continuous time.

the closed-loop response of the system when subjected to a 0.1-second delay in the sensor feedback channel.

The system is stable in the absence of a quantizer or lossy channel, but the QLH, QLF, QLZ, and Q blocks introduce limit cycles at specific amplitudes and frequencies. These limit cycles occur at significantly different quantization levels

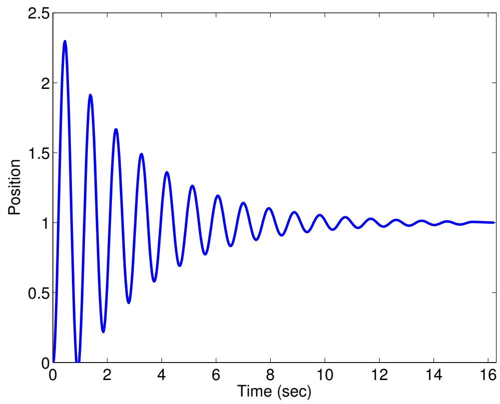

Fig. 14: Closed-loop step response of example system in continuous time when subjected to 0.1-second delay in sensor feedback channel.

depending on the system, and not all limit cycles occur in every system.

To find limit cycles in these four systems we vary the quantization bin size h, which in turn modifies the packet loss probability α through the parameter m. We then determine which nondimensional input frequency and gain lead to limit cycling, defined as when the Nyquist plot of the loop transfer function passes through the point (-1,0). Figure 15 shows resulting limit cycles predicted by the DF models for all four scenarios as a function of quantization level h.

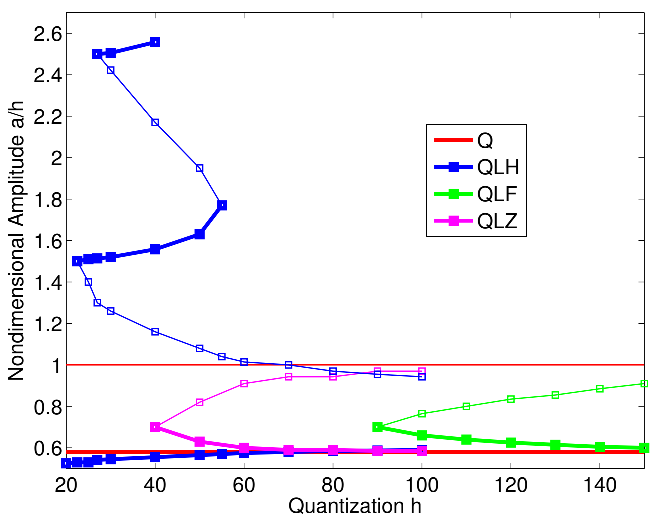

Fig. 15: Plot of nondimensional input amplitude a/h and quantization level h that result in a limit cycle in the example system. Plots are made for a system with QLH, QLF, QLZ, and Q block. Thick lines represent stable limit cycles and thin lines represent unstable limit cycles.

Figure 15 shows that if the system had only a quantizer, limit cycles would exist at amplitude ratios a/h=0.58 and 1.0. Interestingly, the QLH introduces limit cycles (shown by the blue lines) at values of a/h at 0.5 and between 0.95 and 2.6, depending on quantization level . This is because the DF's for both the lossy channel plus hold-input decoder and the quantizer affect the gain. For a fixed value of h the lossy channel plus hold-input decoder DF gain will be fixed, but the quantizer gain will depend on a/h. We've limited this analysis to limit cycles with nondimensional amplitude less than or equal to 2.6 in the case of the QLH system, though higher-amplitude limit cycles do exist.

The QLZ introduces similar limit cycles as Q for large values of parameter h, but limited to $h > 40$. QLF also produces similar limit cycles as Q model, but only for $h > 90$. As h increases, the QLF, QLZ, and QLH limit cycle curves approach the values of the pure quantization curves as expected, because at coarse quantization the quantizer should dominate the system.

We next determine the stability of all limit cycles. We use the limit cycle stability criterion [18] that states that the stability is determined by the behavior near the intersection points of the plant Nyquist plot and the negative inverse of the DF Nyquist plot. The stability is represented in Figure 15 with solid lines for stable limit cycles and dashed lines for unstable limit cycles. This analysis shows the Q, QLZ, and QLF systems introduce one stable limit cycle each, while the QLH system introduces three stable limit cycles. It would be important for designers to takes these stable limit cycles into account when designing system controllers and choosing quantization levels. Figure 16 shows the nondimensional frequency and quantization level for the limit cycles. At higher values of quantization level the limit cycle frequencies are similar in Q, QLZ, and QLH cases, though the frequencies are much higher for the QLF case. Closer inspection of the plots reveals multiple limit cycle frequencies at some quantization levels for each branch, corresponding to the different stable and unstable branches of the plots in Figure 15. However, these frequencies are very close in magnitude and practically indistinguishable.

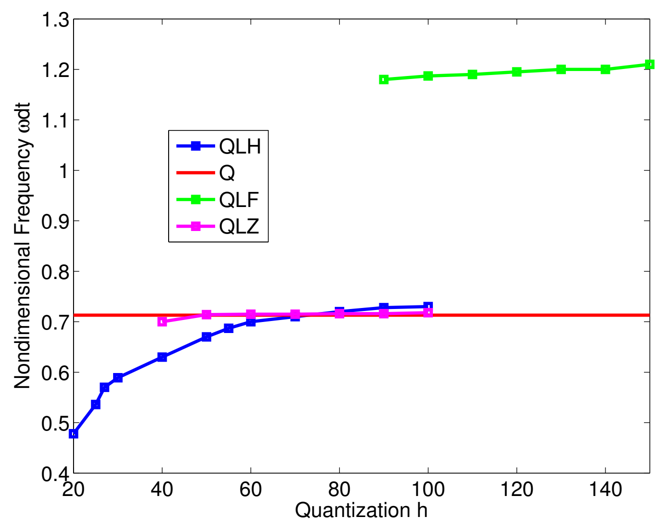

Fig. 16: Plot of quantization level and nondimensional frequency ωdt of limit cycles for Q, QLH, QLF, and QLZ.

VII. Conclusion

We have developed and validated by simulation the closed-form expressions for the DF's of three important systems: QLF, QLH, and QLZ. These are fundamental elements of many robotics and control systems employing wireless communication, and thus our analysis is relevant to current practice. We demonstrate through a simple example how the DF's for a system with QLH, QLZ, or QLF elements predict stable limit cycles at different quantization levels for each scenario. Some stable limit cycles would not be predicted with a quantizer DF alone. The analytic DF equations we derive moreover allow quick performance analysis of different control gains without needing to perform lengthy simulations.

Acknowledgments

Work is supported by the Office of Naval Research, Grant N00014-09-1-0700, the National Science Foundation, Contract CNS-1212597, and Finmeccanica.

References

[1] K. Tsumura, H. Ishii, and H. Hoshina, "Tradeoffs between quantization and packet loss in networked control of linear systems," *Automatica*, vol. 45, no. 1, pp. 2963–2970, 2009.

[2] Y. Niu, T. Jia, X. Wang, and F. Yang, "Output-feedback control design for ncss subject to quantization and dropout," *Information Sciences*, vol. 179, no. 1, pp. 3804–3813, 2009.

[3] M. Liu, Q. Wang, and H. Li, "State estimation and stabilization for nonlinear networked control systems with limited capacity channel," *Journal of the Franklin Institute*, vol. 348, no. 1, pp. 1869–1885, 2011.

[4] J. Dai, "A delay system approach to networked control systems with limited communication capacity," *Journal of the Franklin Institute*, vol. 347, no. 1, pp. 1334–1352, 2010.

[5] F. Rasool and S. Nguang, "Quantised robust h infinity output feedback control of discrete-time systems with random communication delays," *IET Control Theory and Applications*, vol. 4, no. 11, pp. 2252–2262, 2010.

[6] J. Guckenheimer and P. Holmes, "Nonlinear oscillations dynamical systems and bifurcations," *Applied Mathematical Sciences*, vol. 42, 1990.

[7] J. Mallet-Paret and H. Smith, "The poincare-bendixson theorem for monotone cyclic feedback systems," *Journal of Dynamics and Differential EQuations*, vol. 2, no. 4, pp. 367–422, 1989.

[8] M. Basiri, A. Bishop, and P. Jensfelt, "Distributed control of triangular formations with angle-only constraints," *Systems and Control Letters*, vol. 59, pp. 147–154, 2010.

[9] W. Wang and J.-J. Slotine, "On partial contraction analysis for coupled nonlinear oscillators," *Biological Cybernetics*, vol. 92, pp. 38–53, 2004.

[10] A. Gelb and W. Velde, *Multiple-Input Describing Functions and Nonlinear System Design*. [USA] McGraw-Hill, Inc., 1968.

[11] S. Sanders, "On limit cycles and the describing function method in periodically switched circuits," *IEEE Transactions on Circuits and Systems-I: Fundamental Theory and Applications*, vol. 40, no. 9, pp. 564–573, 1993.

[12] A. Peterchev and S. Sanders, "Quantization resolution and limit cycling in digitally controlled pwm converters," *IEEE Transactions on Power Electronics*, vol. 18, no. 1, pp. 301–309, 2003.

[13] E. Kim, H. Lee, and M. Park, "Limit-cycle prediction of a fuzzy control system based on describing function method," *IEEE Transactions on Fuzzy Systems*, vol. 8, no. 1, pp. 11–23, 2000.

[14] D. Yoerger, J. Cooke, and J.-J. Slotine, "The influence of thruster dynamics on underwater vehicle behavior and their incorporation into control system design," *IEEE Journal of Oceanic Engineering*, vol. 15, no. 3, pp. 167–179, 1990.

[15] D. Tang, E. Dowell, and L. Virgin, "Limit cycle behavior of an airfoil with a control surface," *Journal of Fluids and Structures*, vol. 12, no. 1, pp. 839–858, 1998.

[16] N. Noiray, D. Durox, t. Schuler, and S. Candel, "A unified framework for nonlinear combustion instability analysis based on the flame describing function," *Journal of Fluid Mechanics*, vol. 615, no. 1, pp. 139–167, 2008.

[17] E. Riskin, C. Boulis, S. Otterson, and M. Ostendorf, "Graceful degredation of speech recognition performance over lossy packet networks," in *Proc. Eurospeech*, 2001.

[18] J.-J. E. Slotine and W. Li, *Applied Nonlinear Control*. [Upper Saddle River, New Jersey] Prentice Hall, Inc., 1991.